

## Midwinter Deceleration of the Subtropical Mesospheric Jet and Interannual Variability of the High-Latitude Flow in UKMO Analyses

TIMOTHY J. DUNKERTON

*Northwest Research Associates, Bellevue, Washington*

(Manuscript received 3 June 1999, in final form 8 February 2000)

### ABSTRACT

The variability of zonally averaged stratospheric circulation is examined using daily gridded analyses from the U.K. Met. Office for 1991–99, corresponding to the period observed by the *Upper Atmosphere Research Satellite*. Application of rotated principal component analysis to the dataset reveals dominant modes of variability consisting of annual, semiannual, and quasi-biennial oscillations, together with intraseasonal and interannual variability in the winter hemisphere. In the upper stratosphere during northern winter, poleward propagating zonal wind anomalies at the stratopause and a sudden deceleration of the subtropical mesospheric jet in each midwinter are observed. The high-latitude flow is more variable, and the data suggest two contrasting types of wintertime evolution in the polar stratosphere. One is characterized in high latitudes by relatively strong flow in early winter and a significantly weakened flow after solstice, the other by relatively weak flow in early winter and a strong positive flow anomaly after solstice. In both, the subtropical deceleration is accompanied by high-latitude acceleration. In the second type, polar westerlies remain long after solstice, decaying gradually, while in the first type, polar easterlies appear after 10–30 days. In two winters of the first type, the subtropical deceleration is unusually abrupt, followed by brief reacceleration of the polar vortex and a spectacular breakdown after 30 days. Multivariate EOF analysis incorporating temperature data separates deceleration events in northern winter affecting the subtropical jet, with midlatitude warming, from those affecting the polar night jet, with polar warming.

### 1. Introduction

Daily gridded analyses of the troposphere, stratosphere, and lower mesosphere have been produced by the U.K. Met. Office (UKMO) since 1991 (Swinbank and O'Neill 1994) in support of the *Upper Atmosphere Research Satellite* (UARS) mission (Reber et al. 1993). Early observations of UARS dynamical fields and trace constituents, together with UKMO analyses, were discussed in a special issue of the *Journal of the Atmospheric Sciences* (15 October 1994). Today, UKMO analyses are still being produced on a regular basis, and several UARS instruments continue to function, allowing a more rigorous investigation of variability and trends in the middle atmosphere (Randel et al. 1998, 1999a,b; Gray and Russell 1999). The purpose of this paper is to discuss the zonally averaged dynamical variability of the stratosphere as seen in UKMO analyses for 1991–99. A companion paper examines the interannual variability in monthly mean Halogen Occultation Experiment (HALOE; Russell et al. 1993) observations of methane, water vapor, and ozone (Dunkerton 2000).

The elements of the zonally averaged stratospheric circulation—consisting primarily of fluctuations in the zonal velocity component—are relatively simple and have been known for many years. In extratropical latitudes the annual cycle is by far the largest variation, with westerlies in winter and easterlies in summer, while semiannual and quasi-biennial oscillations (SAO and QBO) are observed in the tropical upper and lower stratosphere, respectively (Belmont et al. 1974, 1975; Andrews et al. 1987). Annual and semiannual cycles compose the seasonal climatology, while the QBO (centered on the equator) is the dominant mode of interannual variability in the tropical lower stratosphere. Intraseasonal variability is observed primarily in winter, due to major or minor warmings (Labitzke 1981) and their associated mean-flow deceleration. The variability is larger in northern winter, due to more intense planetary wave activity in this hemisphere. The SAO is not exactly semiannual but displays seasonal variation, with a stronger first cycle in the calendar year as expected from the hemispheric asymmetry of wave driving; the SAO is also modulated by the underlying QBO (Garcia et al. 1997; Dunkerton and Delisi 1997). The QBO is thought to modulate the extratropical mean circulation (Holton and Tan 1980) via changes in planetary wave activity (Dunkerton and Baldwin 1991; O'Sullivan and Dunkerton 1994) so that the low- and high-latitude com-

---

Corresponding author address: Dr. Timothy J. Dunkerton, Northwest Research Associates, P.O. Box 3027, Bellevue, WA 98009-3027.  
E-mail: tim@nwra.com

ponents of stratospheric variability are not independent, but loosely connected. As discussed in the companion paper and references therein, stratospheric trace constituents are affected significantly by the seasonal and QBO variations and their nonlinear interaction.

In recent years the techniques of principal component analysis (PCA) and singular value decomposition (SVD) have proven useful in the investigation of the stratospheric circulation and trace constituent behavior. Coupling of the polar troposphere and lower stratosphere was observed in northern winter as a leading empirical orthogonal function (EOF) or SVD mode (Baldwin et al. 1994) also known as the Arctic Oscillation (Thompson and Wallace 1998, 2000). Interaction between the annual cycle and the QBO was found in the stratosphere by examining the frequency spectrum of the leading principal component of angular momentum (Baldwin and Tung 1994). Randel et al. (1998) used SVD to examine the covariance of QBO and HALOE trace constituents, while the trend of HALOE methane was contained in the leading unrotated EOF of this constituent (Randel et al. 1999a). Horizontal patterns of column ozone variability in Total Ozone Mapping Spectrometer (TOMS) data were derived as rotated EOFs by Eder et al. (1999). Extended SVD modes were used by Kuroda and Kodera (1999) to identify propagating patterns in mean-flow and planetary wave fluxes.

Objective analysis techniques such as PCA, SVD, and canonical correlation analysis—used extensively in the atmospheric sciences—provide a compact description of the spatial distribution of temporal variance or covariance of gridded data, identifying the dominant modes of variability (Bretherton et al. 1992; Kim and Wu 1999, and references therein). Orthogonal rotation of spatial EOFs and their associated time series or “principal components” yields physically meaningful patterns among higher modes when several types of variability are present (Cheng and Dunkerton 1995; Livezey and Smith 1999). As shown herein, varimax rotation allows the simultaneous identification of climatological, intraseasonal, and interannual variations of the zonally averaged circulation of the stratosphere. Dominant elements of variability, therefore, can be determined objectively without a priori specification of their spatial or temporal dependence. The rotated EOF description is surprisingly efficient, compressing the effective size of the dataset by approximately 2 orders of magnitude. More important, results obtained from the analysis provide new insights into stratospheric behavior. Our approach is similar to that of Nigam (1990) but will focus on the stratosphere, including the upper stratosphere where (apart from the QBO) variance is largest.<sup>1</sup>

<sup>1</sup> The increase of variance with altitude continues into the lower mesosphere, but for various reasons our analysis of UKMO data will be restricted, for the most part, to stratospheric levels.

## 2. Data analysis

Zonally averaged zonal wind and temperature were obtained from daily UKMO data. The latitudinal resolution is 2.5°, with 22 levels spaced uniformly in log pressure from 1000 to 0.316 hPa. Results obtained with temporal filtering used a triangle filter of half-width 23 days, having a frequency response nearly identical to that of a 30-day running mean but without the sidelobes of a running mean. The low-pass filtering is therefore similar to that of a conventional monthly mean but without the constraint that anomaly extremes occur at mid-month. Lightly filtered data, obtained with a half-width of 5 days, were also used in the analysis of intraseasonal variability. Unrotated EOFs were derived as eigenfunctions of the temporal covariance matrix. Rotated EOFs and principal components were obtained using varimax rotation. For multivariate EOFs of zonal wind and temperature, each field was normalized by its global standard deviation, yielding a nondimensional covariance matrix with approximately equal weighting of each quantity. The data record used in the analysis extends from 17 October 1991 through 13 November 1999.

## 3. Principal components

### a. Variance of mean zonal wind

A latitude–height cross section of the time-mean, zonally averaged zonal wind in the stratosphere is shown in Fig. 1a. The time-mean flow is characterized by westerlies poleward of 30° and easterlies in the Tropics. A tiny pocket of weak westerlies exists in the lowermost equatorial stratosphere, as found in rawinsonde data. Time-mean westerlies are much stronger in the Southern Hemisphere due to stronger westerlies in the southern winter season. Asymmetry is also seen in the temporal standard deviation of zonally averaged zonal wind, shown in Fig. 1b. Values of  $\sigma(\bar{u})$  are about twice as large in the southern lower stratosphere and about 50% larger in the southern upper stratosphere. The quasi-biennial oscillation is responsible for a separate variance maximum centered on the equator at 22 hPa. Above this level, a variance minimum in UKMO data is found on the equator at 4.6 hPa. The standard deviation of low-pass filtered data, shown in Fig. 1c, is almost identical to that of unfiltered data. The standard deviation of high-pass filtered data (defined as the difference between unfiltered and low-pass filtered data) accounts for the remaining variance and consists in each hemisphere of a deep maximum in high latitudes and a broad shelf in the upper stratosphere extending into subtropical latitudes, as shown in Fig. 1d. The pattern is asymmetric with values in the Northern Hemisphere about 50% larger. Apart from the QBO, variance increases uniformly with height in each of the figures.

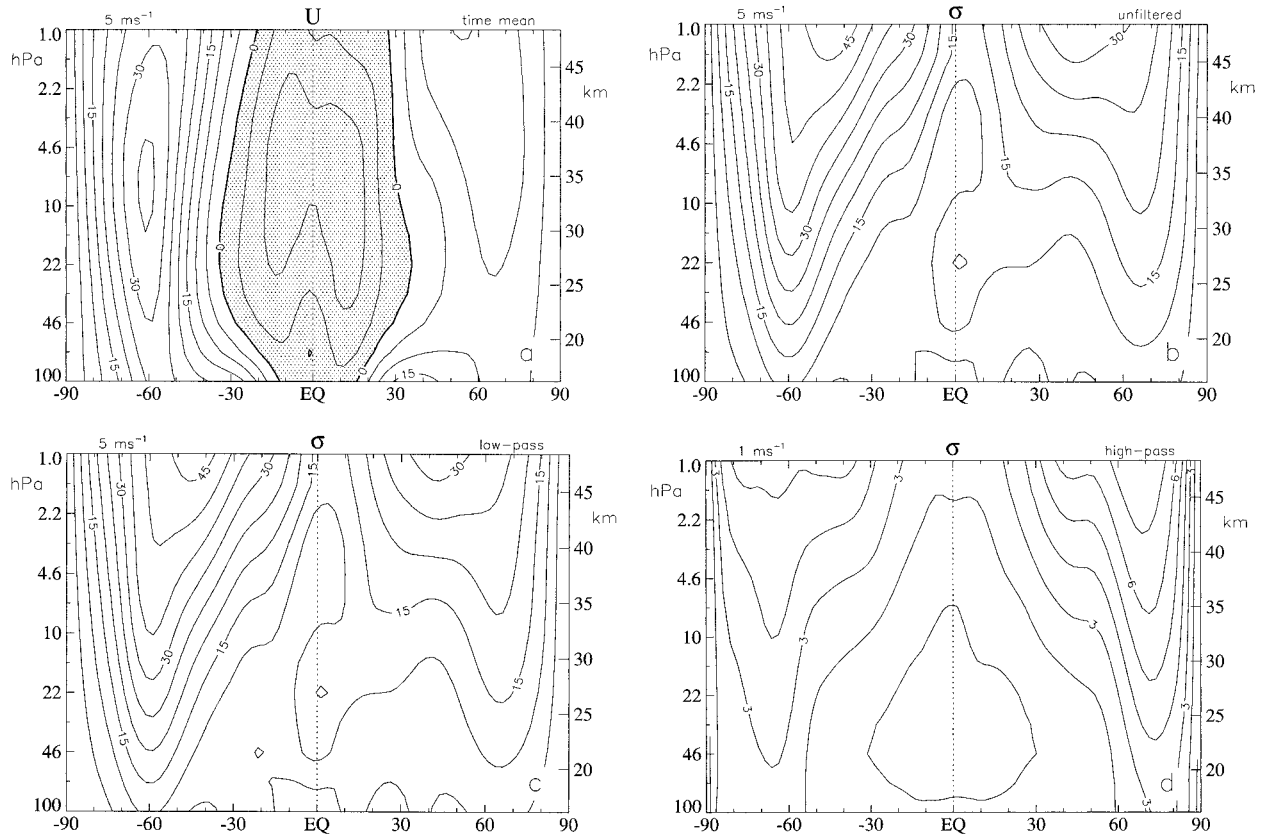


FIG. 1. Mean zonal wind statistics derived from UKMO data for 1991–99. (a) Time mean of zonally averaged zonal wind. Shading indicates negative values. (b), (c), (d) Standard deviation of zonally averaged zonal wind for unfiltered, low-pass, and high-pass filtered data.

### b. Principal components of unfiltered data

The first 10 rotated EOFs of unfiltered zonally averaged zonal wind are shown in Fig. 2, normalized to unit variance. Twelve modes were rotated (out of a possible 936, the number of stratospheric grid points) of which only the first 10 display simple structure and appear to be physically meaningful. These 10 modes account for 97.4% of the total variance in the stratosphere. An acronym for each mode identifies something about the spatial structure of the EOF, or temporal dependence of the associated principal component time series shown in Fig. 3 (also normalized to unit variance). These series, after low-pass filtering, are almost identical to the principal components derived from low-pass filtered data (not shown).

**Annual cycle.** The first mode explains 76.9% of the unfiltered variance and is similar to the distribution of total variance, but with a broad extratropical maximum in each hemisphere and lacking the QBO component (Fig. 2a). The structure is antisymmetric about the equator but not exactly so, with Southern Hemisphere weightings about twice as large as those in the Northern Hemisphere. The maximum amplitude occurs at the solstices and is nearly identical from year to year. This

dominant structure accounts for winter westerlies and summer easterlies in both hemispheres.

**Semiannual oscillation.** The second mode, unlike the first, is roughly symmetric about the equator but with somewhat larger amplitude south of the equator (Fig. 2b). The temporal variation is a fairly regular semiannual oscillation. Maximum positive values occur at or shortly after the solstices, accounting for the easterly phase of the semiannual oscillation in the tropical and subtropical upper stratosphere. The stratopause SAO in UKMO data was described by Ray et al. (1998).

**Annual, with maximum at equinox.** The third mode has largest amplitude in the southern middle stratosphere (Fig. 2c) and is characterized by a somewhat skewed time series with maxima in Southern Hemisphere spring. This structure accounts for the extended duration of the westerly polar vortex in the southern winter/spring season, responsible for conditions leading to ozone depletion above Antarctica. There is an anomaly of opposite sign aloft, indicating deceleration in the midlatitude upper stratosphere during this time. There is also a weak positive maximum in the north polar upper stratosphere, associated with negative anomaly values in northern spring, implying a relatively earlier destruction of the polar vortex compared to that of the

Southern Hemisphere. It is interesting that these two signals are combined in a single rotated EOF even though they are dynamically unrelated. When principal component analysis is applied to climatological variations, spatially separated phenomena sharing a common temporal variation may appear together in the same EOF (Weickmann and Chervin 1988).

*Polar night jet monopole.* Intraseasonal variance associated with the polar night jet (PNJ) in northern winter is contained in the fourth mode (Fig. 2d), centered near 65°N. The time series is irregular with large swings in the northern winter season. One or two positive maxima are observed in each winter, corresponding to deceleration of the polar upper stratosphere.

*Subtropical mesospheric jet monopole.* Intraseasonal variance associated with the subtropical mesospheric jet (SMJ) in northern winter is contained in the fifth mode (Fig. 2e), centered between 30° and 40°N and extending slightly across the equator in the upper stratosphere. The time series is irregular with large swings in the northern winter season. Some regular behavior is seen, with a large positive spike at each northern winter solstice, surrounded by negative values on either side. Positive extremes, corresponding to a strong easterly anomaly, occur as a result of sudden deceleration of the subtropical mesospheric jet, previously observed in December 1978 by the Limb Infrared Monitor of the Stratosphere (Dunkerton and Delisi 1985a). It is noteworthy that this event occurs in each winter of the UKMO observing period, although with different timing (some slightly before solstice, and others slightly after). This observation indicates that the smooth acceleration of the subtropical mesosphere jet in early winter leads to what might be regarded as an unstable situation, subject to sudden deceleration and a more chaotic evolution thereafter.

*Semiannual oscillation, Southern Hemisphere.* The sixth mode represents semiannual variance in quadrature with the second mode, combining the westerly phase of the tropical SAO with a stronger semiannual variation in the upper stratosphere of the Southern Hemisphere (Fig. 2f). Positive maxima occur near equinoxes, consistent with phase descent of the tropical SAO. In UKMO data the tropical SAO is somewhat weak, however, in comparison to the real SAO (Hitchman and Leovy 1986; Garcia et al. 1997; Dunkerton and Delisi 1997), and this weakness is seen in the unremarkable tropical signature of the rotated EOF. Instead we find a horizontal dipole at the southern stratopause, contributing to a transient deceleration of the south polar vortex in midwinter. There is no obvious dynamical link between the tropical and extratropical components of this mode.

*Quasi-biennial oscillation monopole.* The seventh mode accounts in part for an isolated variance maximum associated with the stratospheric QBO (Fig. 2g), centered on the equator near 22 hPa. The time series, even in unfiltered data, is remarkably devoid of high-frequency

variance. The QBO period is 24–27 months, with indication of QBO phase progression through the calendar year, that is, periods longer than 24 months.

*Polar night jet dipole.* Variability of the north polar vortex in the middle stratosphere is contained in the eighth mode (Fig. 2h) with opposite phase in the mid-latitude middle stratosphere and polar upper stratosphere. The time series is irregular with large swings in the northern winter/spring season.

*Quasi-biennial oscillation dipole.* Downward propagation of the QBO is implied by the ninth mode (Fig. 2i) when combined with the seventh mode; the time series of the QBO dipole lags that of the monopole by a quarter-cycle. In the first two cycles the transition to easterlies near 15 hPa occurs in northern spring. The role of laterally propagating planetary waves in the easterly phase onset in the middle stratosphere was discussed by Ortland (1997).

*Subtropical mesospheric jet dipole.* The 10th mode corresponds to a horizontal dipole (Fig. 2j) on either side of the SMJ monopole (Fig. 2e). The time series is irregular with large swings in the northern winter season. Close inspection of Fig. 3 reveals that the SMJ dipole extrema in northern winter lead those of the SMJ monopole, typically by a month or less, implying poleward propagation of mean zonal wind anomalies along the Northern Hemisphere stratopause. This feature is discussed in section 5b.

In summary, the rotated EOFs of unfiltered data consist of three pairs representing oscillations (annual, semiannual, and quasi-biennial) together with two pairs of modes representing variability in the winter/spring season of the Northern Hemisphere. Monopoles in general may represent fluctuations in the strength of a zonal jet, while dipoles may represent fluctuations in the position of the jet axis (Nigam 1990). In our case, monopoles and dipoles in quadrature also represent propagating features, either vertically (as in the QBO region) or horizontally (as in the upper stratosphere).

### c. Other results

Almost identical results were obtained with low-pass filtering, with greater percentage of variance in the low-frequency QBO modes. The order of filtered modes is indicated along the right edge of Fig. 3 and this numbering scheme 0, 1, . . . , 9 will be used in the remainder of the paper.

Results with the three mesospheric levels included were also similar, with one exception. The SMJ monopole acquired some variance associated with the semiannual oscillation; the SAO mode was diminished in variance and relegated to the southern subtropics. Their time series (not shown) indicate that the modified SMJ-m mode is no longer associated primarily with the stratopause deceleration described above (although these events are still contained in the time series). Instead the time series is quite regular and contains var-

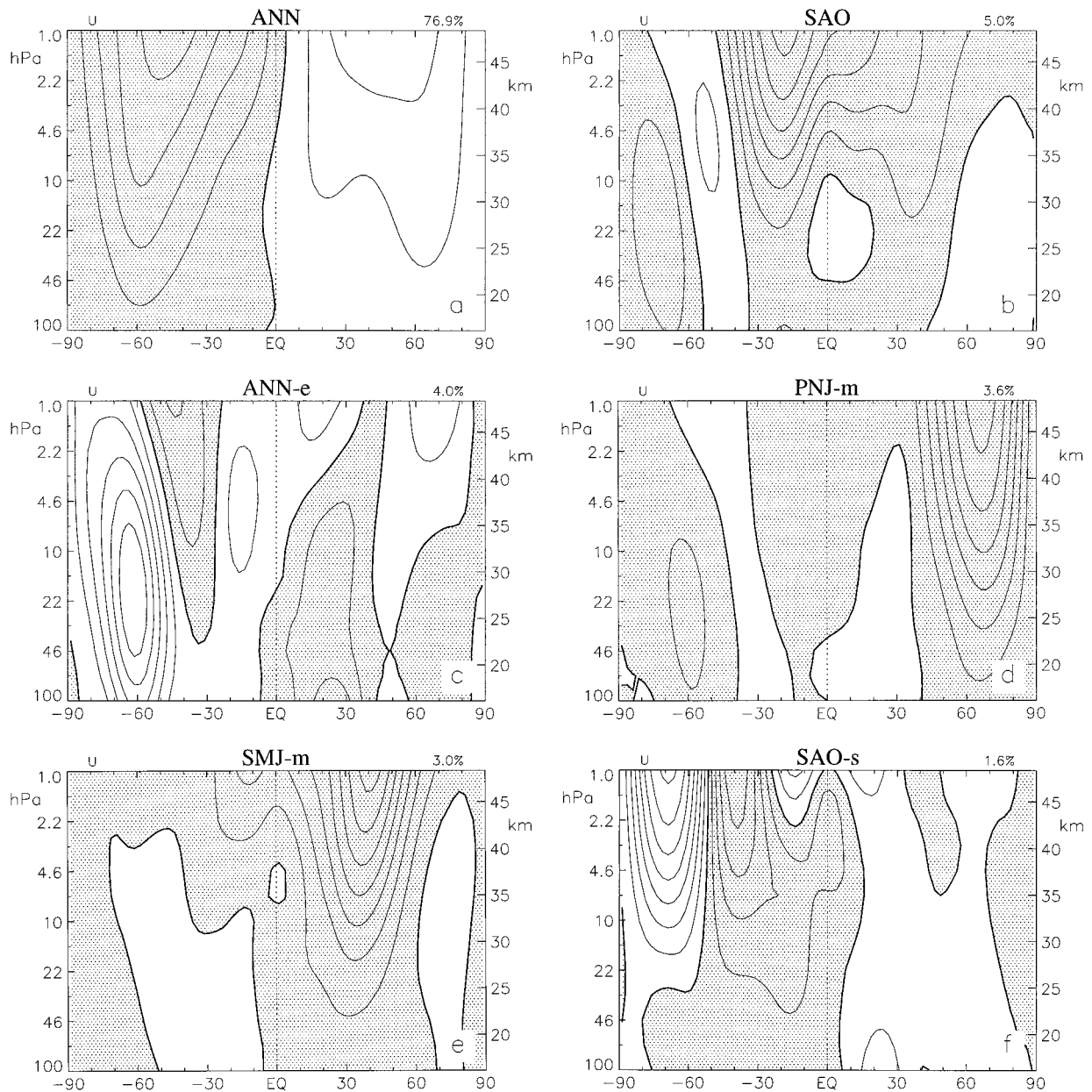


FIG. 2. Rotated EOFs of zonally averaged zonal wind from unfiltered UKMO data, normalized to unit variance. Shading indicates negative values.

iance associated with both the first and second cycles of the tropical SAO.

Temporal correlations of principal components obtained with and without the three mesospheric levels are arrayed in the top half of Table 1. Each mode of stratospheric data has its counterpart in the combined stratosphere–mesosphere dataset, except for the rearrangement of SAO variance described above. As to which of these representations is more meaningful (with or without mesospheric levels) is difficult to determine. The overall similarity is not a good sign, suggesting that little independent information has been added with me-

ospheric levels included. These levels, located near the top of the assimilation model, may be constrained to behave unrealistically. The alteration of SMJ-m mode is detrimental for the purpose of describing the stratospheric deceleration in northern winter. This is clearly an intraseasonal event—rapidly evolving, and somewhat variable in its timing—not part of the climatological SAO.

Similar results were again obtained in multivariate EOFs of mean zonal wind and temperature. Only stratospheric levels were used in the calculation due to problems with mesospheric temperature data (spurious dis-

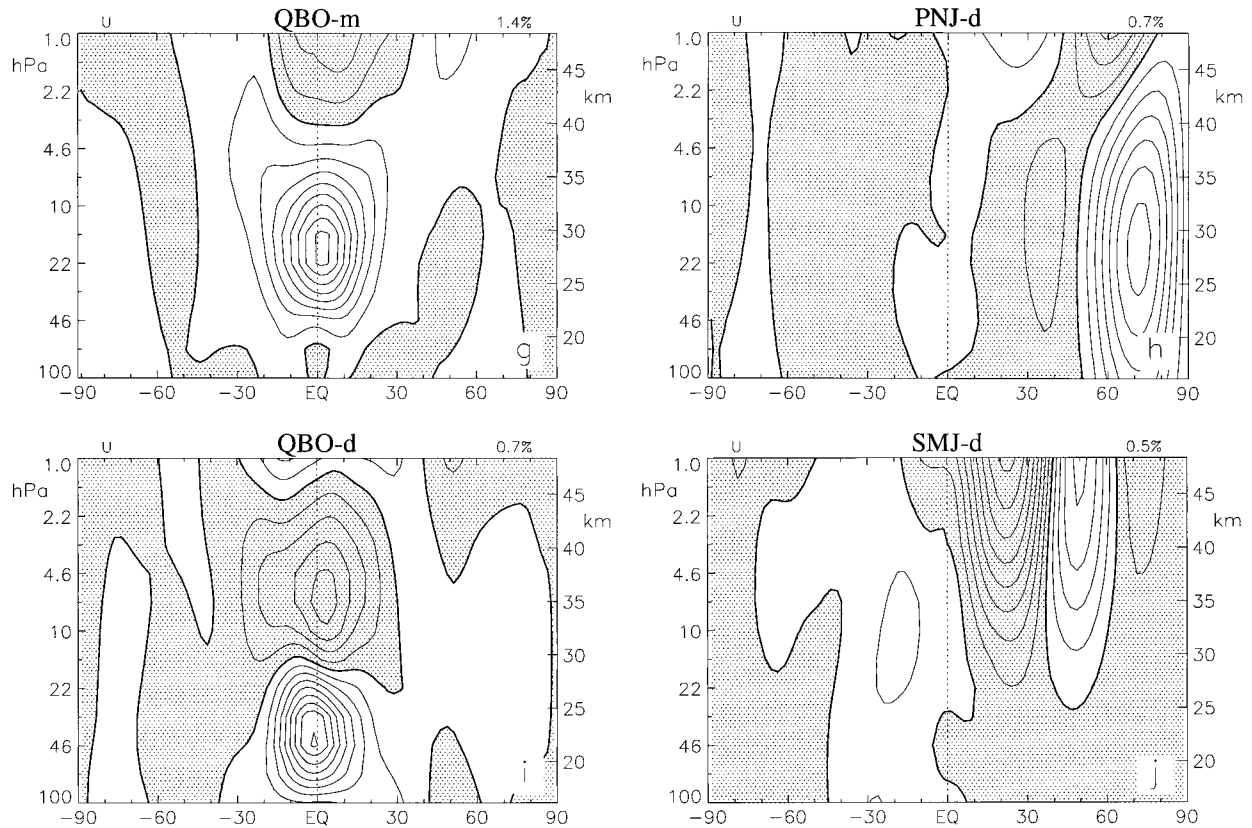


FIG. 2. (Continued)

continuities and trend). The calculation was computationally intensive, involving a  $1885 \times 1885$  covariance matrix at double precision. To give equal weight to zonal wind and temperature, the two fields were normalized by their global standard deviation ( $19.7 \text{ m s}^{-1}$  and  $10.6 \text{ K}$ , respectively). As shown in the bottom half of Table 1, each of the original modes has its counterpart in the multivariate analysis, with the possible exception of the polar night jet dipole, which acquired some variance from the SMJ-m mode and is characterized by strong temperature fluctuations in the north polar upper stratosphere. This alteration benefits the SMJ-m mode, which retains its intraseasonal character and has a spatial structure more tightly confined to the subtropical mesospheric jet (not shown). The corresponding temperature anomaly indicates warming of the northern midlatitude upper stratosphere and cooling in the tropical upper stratosphere. During deceleration events, the mean meridional circulation responsible for temperature anomalies in the PNJ-d and SMJ-m modes would be characterized by subsidence in the polar and midlatitude stratosphere, respectively, and upwelling in a broad region extending across the equator. The time series indicates a preference for subtropical deceleration near the northern winter solstice and midlatitude deceleration after the solstice.

Apart from a globally averaged temperature fluctuation, the inclusion of temperature in the calculation does not add independent information because the mean zonal wind and temperature are in gradient balance, even for tropical QBO and SAO. The weighting of EOFs can be changed, however, depending on the magnitude of temperature fluctuation, which depends, in turn, on the vertical shear and/or latitude of the EOF. One mode, designated LMT for lower mesosphere temperature trend, corresponds to a (probably spurious) signal of global extent. Each of the other EOFs has a temperature anomaly qualitatively in accord with gradient wind balance.

#### 4. Reconstruction of mean zonal wind

The standard deviation of zonally averaged zonal wind associated with the first 10 modes of low-pass filtered data (not shown) indicates that annual and semi-annual oscillations account for most of the variance, while Northern Hemisphere intraseasonal variability and the quasi-biennial oscillation explain the remainder. On the equator, the amplitude of the QBO grows with height realistically to 22 hPa. Above this level, QBO amplitude decays too rapidly in comparison to that of rocketsonde data (Dunkerton and Delisi 1997). While

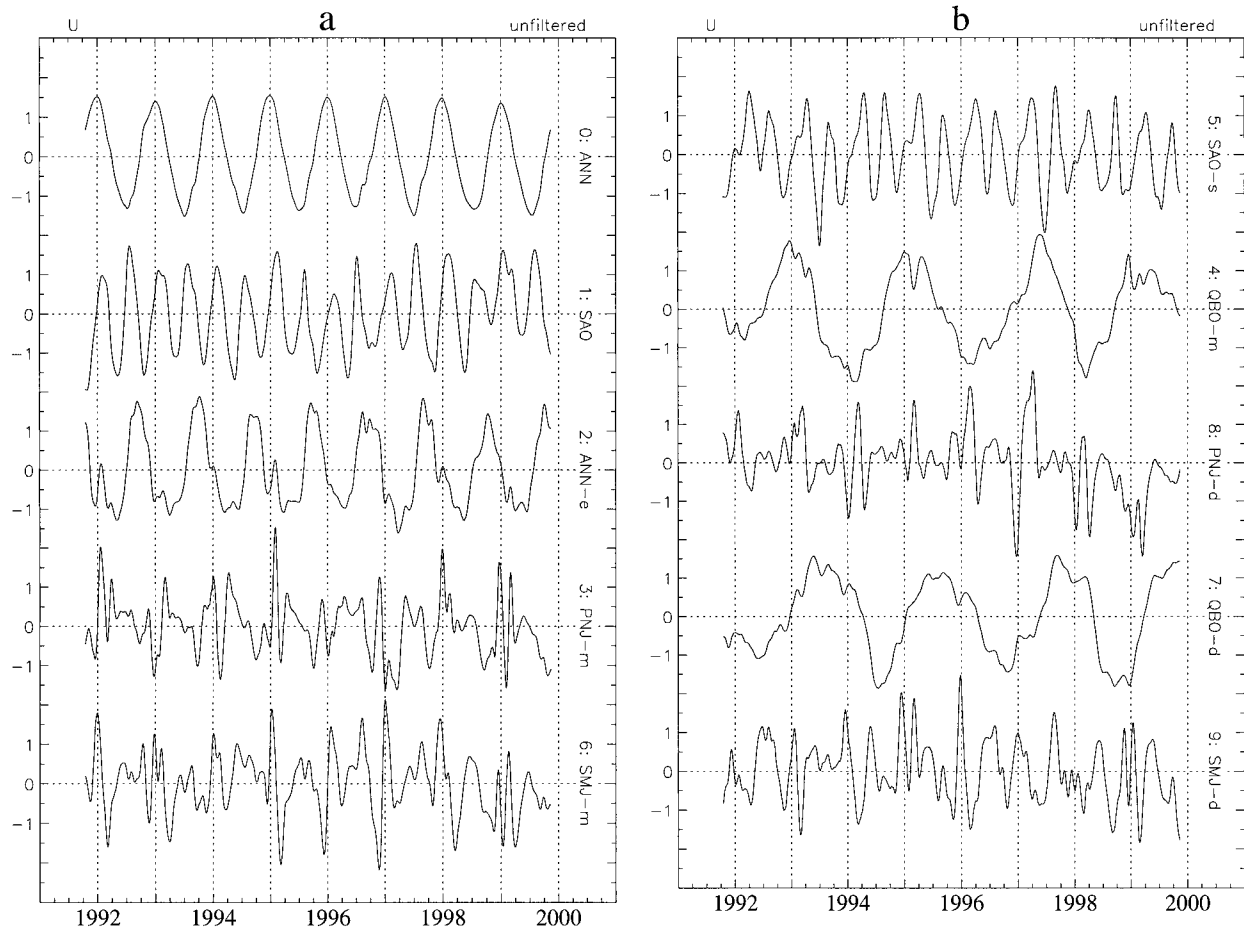


FIG. 3. Principal component time series, after low-pass filtering, corresponding to the rotated EOFs derived from unfiltered data, normalized to unit variance. The order of filtered EOFs is indicated at right.

the UKMO assimilation seems to be correctly constrained by rawinsonde observations of the QBO, these measurements generally do not extend high enough to capture the entire QBO. Derivation of equatorial wind from routine satellite temperatures is problematic due to the vanishing Coriolis parameter and coarse vertical resolution of the satellite data, and rocketsonde observations are no longer routinely acquired. It should be possible to improve the assimilation's near-equatorial winds using High Resolution Doppler Imager data from *UARS* (D. Ortland 1999, personal communication); however, these data do not sample the stratopause region and are not available in all months.

Reconstruction of mean zonal wind using a partial sum of rotated EOFs multiplied by their respective principal component time series provides an overview of the flow evolution throughout the *UARS* observing period and illustrates the role of the various EOF modes, as shown in Figs. 4a–c. These illustrations were derived from low-pass filtered data, and it should be kept in mind that the filtering eliminates much of the day-to-day variability. This variability, if included, would transform the wintertime areas of these plots into an unde-

cipherable mass of contours when compressed in time to this aspect ratio. Figures 4a–c display the stratopause flow at 1.0 hPa. Figure 4a shows a reconstruction using the 10 leading modes; the percent variance explained on a particular grid level is indicated on the title row. Almost all of the variance at this level is explained by the first 10 modes, and Fig. 4a is almost indistinguishable from the original low-pass filtered data.

At the stratopause, maximum easterlies are found in the subtropics near summer solstice, while maximum westerlies occur in the subtropics and midlatitudes before winter solstice. Westerlies in northern winter are quite variable and the pattern varies from year to year. Each winter has westerlies in early winter, followed by abrupt deceleration in midwinter, and reestablishment of westerlies (to varying degrees) in late winter. The first axis of maximum westerlies propagates poleward from the Tropics to midlatitudes, as does the region of rapid deceleration. By contrast, the high-latitude flow is punctuated by one or two decelerations in each winter, without latitudinal propagation of the signal. In some winters (e.g., 1991/92, 1993/94, 1994/95, 1997/98, 1998/99) the mid- and high-latitude decelerations link

TABLE 1. Temporal correlation of principal component time series derived from an unfiltered stratospheric dataset and a time series of datasets (a) with mesospheric levels included, and (b) with temperature included.

Mode	ANN	SAO	ANN-e	PNJ-m	SMJ-m	SAO-s	QBO-m	PNJ-d	QBO-d	SMJ-d
a) CORR: U vs U_meso										
ANN	<b>0.99</b>	0.08	0.05	-0.01	0.01	0.02	0.00	0.00	-0.01	-0.01
SMJ-m+	-0.05	<i>0.44</i>	-0.04	0.00	<b>0.87</b>	-0.02	0.04	-0.08	-0.06	-0.16
PNJ-m	0.00	0.11	0.00	<b>0.93</b>	0.00	0.01	-0.04	0.24	0.06	0.07
ANN-e	-0.06	0.04	<b>0.99</b>	-0.03	0.02	-0.03	0.00	0.03	0.00	0.00
SAO-s	-0.04	0.28	0.03	-0.04	-0.13	<b>0.93</b>	-0.02	-0.01	-0.05	0.01
SAO-	-0.05	<b>0.81</b>	-0.05	-0.09	-0.38	-0.29	-0.01	-0.01	-0.12	0.18
QBO-m	0.00	0.02	0.01	0.01	-0.04	0.01	<b>0.98</b>	0.01	0.15	0.03
PNJ-d	0.00	0.03	-0.06	-0.30	0.10	0.02	-0.02	<b>0.91</b>	0.07	0.07
QBO-d	0.00	0.17	0.02	-0.03	-0.04	0.00	-0.14	-0.06	<b>0.92</b>	-0.16
SMJ-d	0.01	-0.05	0.02	-0.05	0.19	0.00	-0.07	-0.09	0.13	<b>0.81</b>
b) CORR: U vs UT										
ANN	<b>0.99</b>	-0.02	0.09	-0.04	-0.03	-0.06	0.01	0.01	0.00	0.02
ANN-e	-0.10	0.01	<b>0.95</b>	-0.17	0.09	-0.11	0.01	0.05	0.00	0.04
SAO	0.03	<b>0.98</b>	0.01	-0.01	0.08	0.07	-0.01	-0.13	-0.04	-0.05
PNJ-d+	0.03	0.09	-0.08	0.34	0.52	-0.05	0.00	<b>0.58</b>	0.14	0.16
PNJ-m	0.01	-0.03	0.18	<b>0.90</b>	-0.07	-0.08	0.01	-0.34	-0.04	-0.03
SAO-s	0.04	-0.07	0.14	0.07	0.06	<b>0.95</b>	0.00	0.04	0.03	-0.01
SMJ-m	0.02	-0.13	-0.04	-0.12	<b>0.77</b>	-0.06	0.04	-0.34	-0.03	-0.41
QBO-m	-0.01	0.02	-0.01	-0.01	-0.04	0.01	<b>0.99</b>	0.02	0.04	0.01
LMT	0.00	-0.03	0.02	0.02	0.04	-0.03	0.07	0.12	-0.11	-0.10
QBO-d	-0.01	0.02	0.02	-0.01	-0.04	-0.03	-0.03	-0.07	<b>0.98</b>	-0.06
SMJ-d	-0.01	-0.03	-0.01	-0.04	0.29	-0.04	0.01	-0.10	-0.02	<b>0.79</b>

up, while in other winters (e.g., 1992/93, 1995/96, 1996/97) they do not, as strong westerlies persist through the solstice. The former winters are characterized in high latitudes by relatively strong flow in early winter and relatively weak flow in midwinter. The latter winters are characterized in high latitudes by relatively weak flow in early winter and relatively strong flow in midwinter.

Interannual variability in the Southern Hemisphere is much smaller. Transient deceleration before winter solstice is a regular feature poleward of 60°S. Strong westerlies persist through every solstice, with poleward propagation of the jet axis in the upper stratosphere. The deceleration after this time is comparable to that of northern winter. In tropical latitudes the upper-stratospheric flow is mainly semiannual, although with weaker westerlies than in the real SAO. This is in contrast to the middle stratosphere (not shown) where the QBO is dominant and its easterly phase lasts longer than the westerly phase.

Removal of intraseasonal modes in the Northern Hemisphere eliminates most of the northern wintertime variability (Fig. 4b). Therefore the modes removed account not only for the missing variability but also for much of the poleward propagation of zonal wind anomalies. Removal of SAO modes (not shown) greatly simplifies the stratopause flow, eliminating most of the equatorial variation, the deceleration of south polar vortex in midwinter, and climatological poleward propagation of final deceleration extending from low latitudes in midwinter to midlatitudes in late winter. Removal of the SAO has little effect in the middle stratosphere where the seasonal cycle is mainly annual. Removal of

QBO modes has little effect at the stratopause where the QBO signal is very small in this dataset (unrealistically so), but the effect in the middle stratosphere is huge, leaving only time-mean easterlies and a weak seasonal cycle.

Figure 4c illustrates the superposition of time-mean flow and SAO modes at the stratopause. Tropical and high-latitude manifestations of the SAO are spatially and temporally separated, and probably represent distinct dynamical mechanisms. In the middle stratosphere (not shown) the QBO is imbedded in time-mean easterlies: the zone of absolute westerlies is narrow, confined to within about 10° of the equator. Further details of the UKMO quasi-biennial oscillation and relation of the QBO to HALOE constituents are given in Dunkerton (2000). The “seasonally adjusted” picture of the QBO is like that simulated in a 2D model (Dunkerton 1997) illustrating what the oscillation might look like in the absence of a seasonal cycle. The UKMO data reveal a tendency for QBO westerlies to appear first at the equator and propagate outward, as seen in rawinsonde data (Hamilton 1984; Dunkerton and Delisi 1985b), while the opposite is true of QBO easterlies. The QBO’s diabatic circulation (Plumb and Bell 1982) contributes to this behavior.

## 5. Intraseasonal and interannual variability

Application of principal component analysis to zonally averaged UKMO data provides an objective definition of rotated EOF modes composing the seasonal cycle and departures from climatology. These EOFs pro-

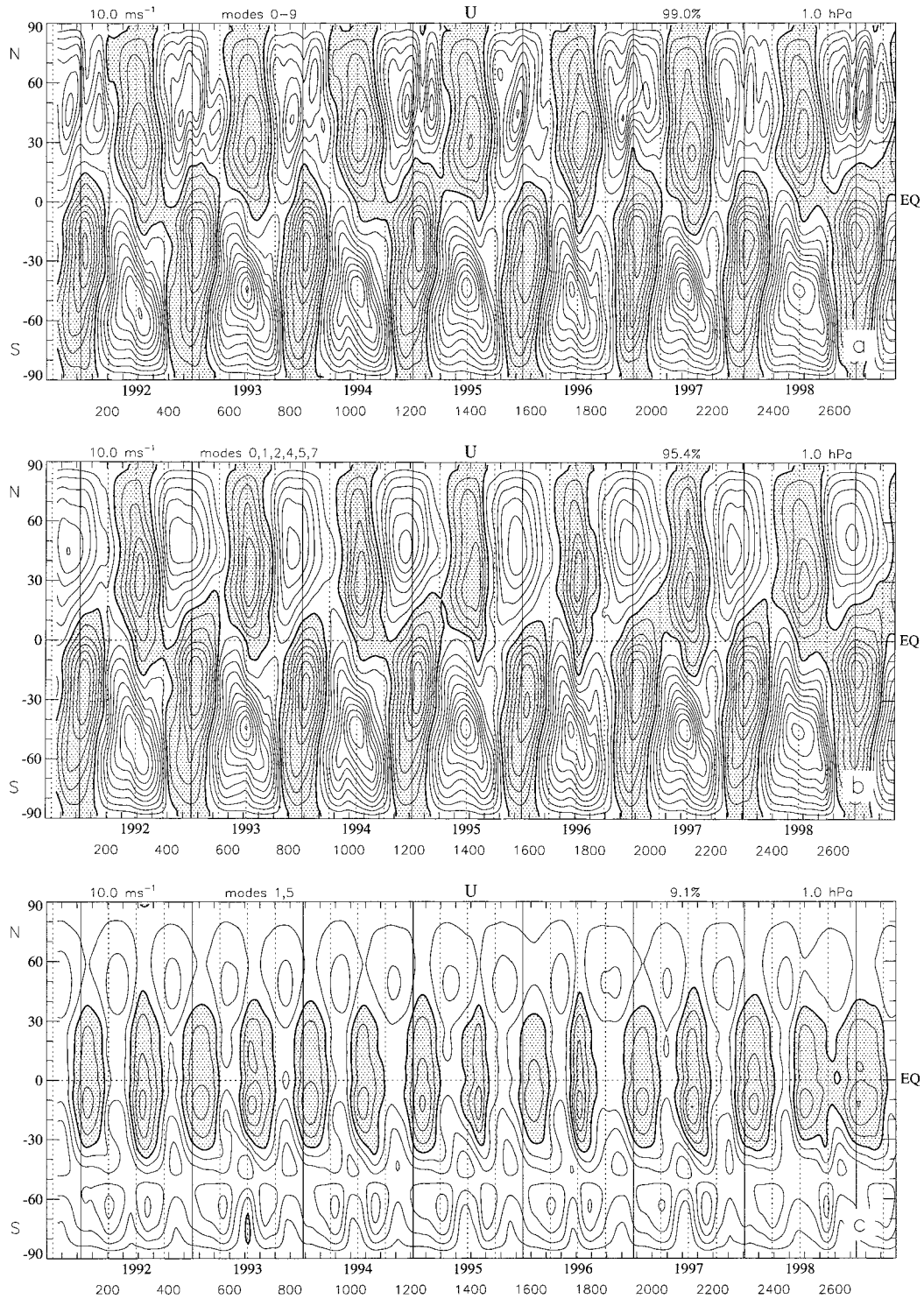


FIG. 4. Time-latitude cross sections of zonally averaged zonal wind obtained from low-pass filtered UKMO data at 1.0 hPa. Shading indicates negative values. (a) Reconstruction of mean zonal wind using the first 10 rotated EOFs multiplied by their respective principal component time series. (b) As in (a), but with Northern Hemisphere intraseasonal modes removed. (c) Superposition of time-mean and SAO modes. Shading indicates negative values; contour interval is  $10 \text{ m s}^{-1}$ .

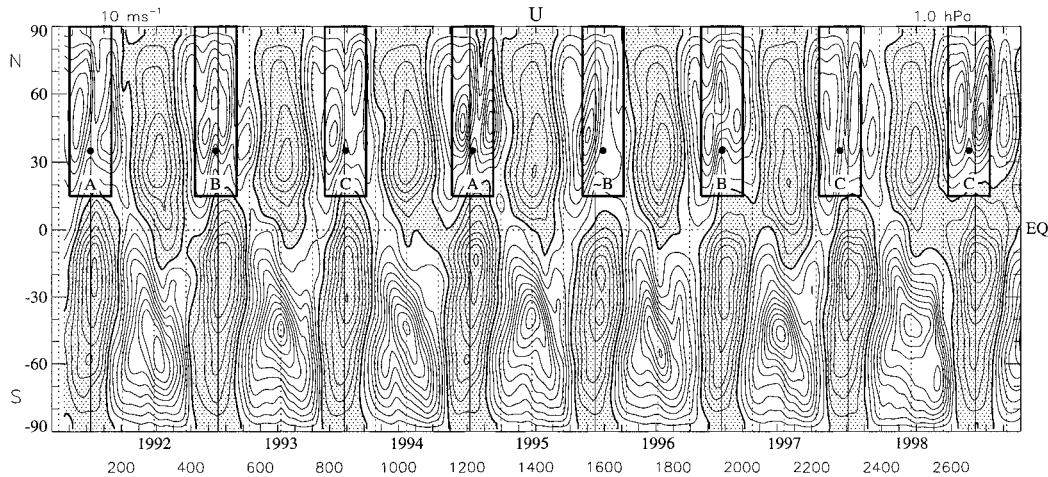


FIG. 5. Time-latitude cross section of zonally averaged zonal wind at 1.0 hPa, from low-pass filtered UKMO data. Large dots indicate the maximum midwinter value of SMJ-m time series, indicating the time of largest easterly anomaly attributable to this mode near northern winter solstice. Boxes show compositing interval. Similar winters are suggested by letters "A," "B," "C." Shading indicates negative values; contour interval is  $10 \text{ m s}^{-1}$ .

vide an optimum statistical explanation of variance, but do not necessarily correspond to dynamical phenomena individually. We have seen in certain cases that separate phenomena sharing a similar temporal variation may appear together in a single EOF. In other cases an EOF may be part of a pair, or larger set of modes, representing phase propagation. In some situations the EOFs may have little meaning at all, as in summer, for example, when variability is weak but the time series of individual modes are nonzero. Not every feature is equally important. The advantage of rotated PCA lies in its inherent flexibility, and efficiency, in defining the spatial and temporal structure of phenomena responsible for most of the variance. The time variation is determined as part of the analysis, allowing key dates to be defined objectively.

#### a. Cluster analysis of northern winters

Deceleration of the subtropical mesospheric jet near northern winter solstice is a regular feature, but not simply a part of the climatology, because its occurrence and subsequent evolution vary somewhat from year to year. The immediate end of deceleration corresponds well to the midwinter positive maximum of SMJ-m time series, indicated by dots in Fig. 5. Recall that the spatial EOF is negative at its core, so that a positive maximum in the time series corresponds to a maximum easterly anomaly. This figure displays the original low-pass filtered data and may be compared to the EOF reconstruction of Fig. 4a. Boxes indicate compositing intervals centered about the SMJ-m maxima, as described momentarily. These intervals lie in midwinter, centered near 1 January, and capture most of the interannual variability of the mid- and high-latitude flow.

The eight winters were classified according to the

evolution of mean zonal wind in the stratosphere from 100 to 1 hPa, using data extending from  $15^{\circ}\text{N}$  to the Pole, within a 121-day window centered on the time of SMJ-m peak amplitude. For this purpose the data were low-pass filtered to remove periods less than about 5 days (hereafter referred to as "lightly filtered" data) giving a more precise time of the midwinter deceleration event. The variability of Fig. 5 is also observed in lightly filtered data, but with more detail: Fig. 6 displays a window of data, centered on the time of SMJ-m peak amplitude, for each of the eight winters. In lightly filtered data, the time of SMJ-m peak is shifted backward by a few days relative to that shown in Fig. 5, due to the asymmetric nature of the time series, that is, gentle acceleration in early winter followed by rapid deceleration in midwinter.

The classification scheme used a simple cluster analysis to combine individual years of winter stratosphere data in such a way as to minimize, at each step, the reduction in the moment of inertia about the average. This is equivalent to minimizing the distance squared between two clusters multiplied by the product of their respective weights. The initial clusters consist of individual winter "maps" in three dimensions, each with 47 190 grid points (121 days, 30 latitudes, 13 pressure levels). Nearby clusters are combined until only two clusters remain. The final cluster obtained by combining the last two is the average of all maps equally weighted. Application of cluster analysis to meteorological data with *time* as one of the dimensions may be novel in this context, but it is also unorthodox, as the number of maps is very small (eight). Reliable results may require a larger sample size. We are motivated by the striking similarity in stratopause data within three sets of winters: (i) 1991/92 and 1994/95; (ii) 1992/93 and 1996/97; (iii) 1993/94, 1997/98, and 1998/99. It is unlikely

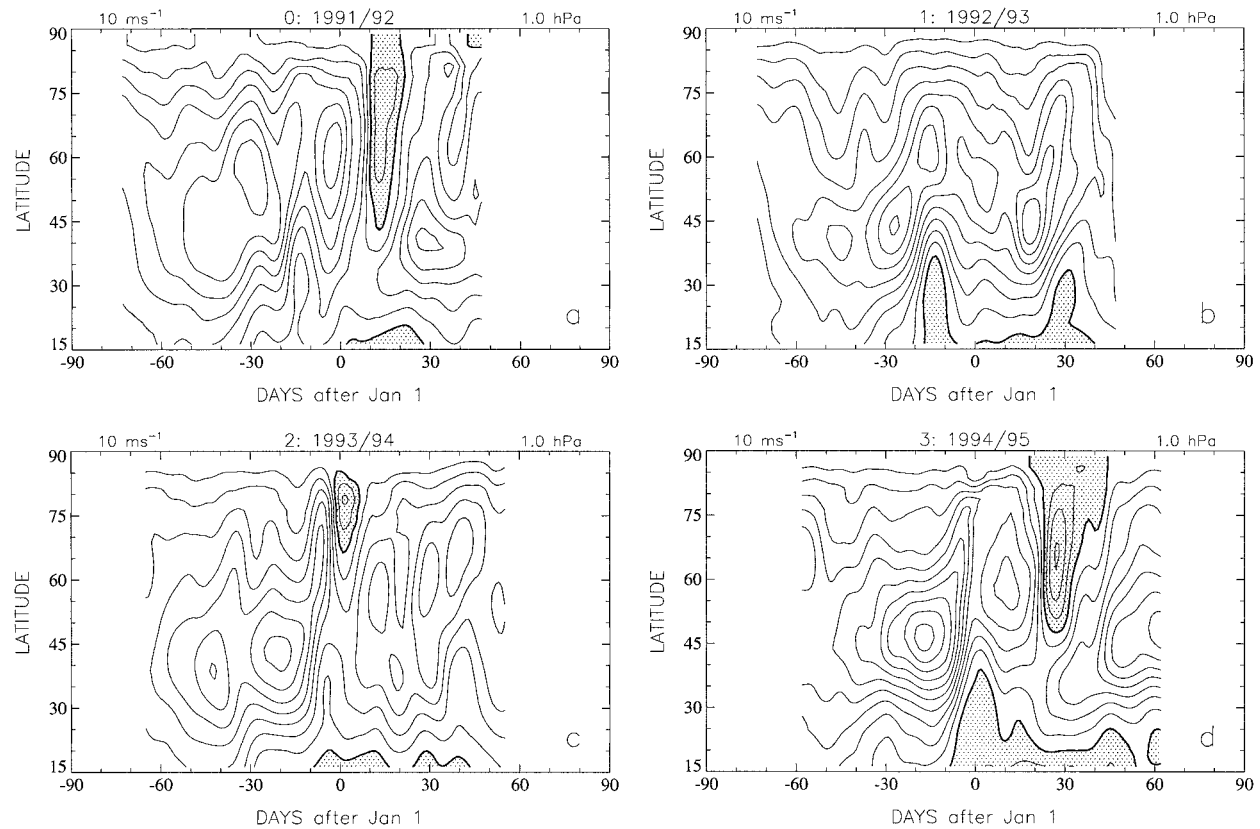


FIG. 6. Time-latitude cross sections of zonally averaged zonal wind at 1.0 hPa, from lightly filtered UKMO data, for each of the eight winters. The 121-day window of data shown corresponds to the time period used in the cluster analysis of Fig. 7, centered on the time of SMJ-m peak amplitude. Shading indicates negative values; contour interval is  $10 \text{ m s}^{-1}$ .

that this resemblance is somehow an artifact of the assimilation model, because the model is constrained to track observations closely from day to day.

The results are summarized in Fig. 7. Two contrasting types of behavior are evident, as noted earlier. The winters 1991/92 and 1994/95 appear similar at this altitude and combine to form the first cluster which will be denoted as “type A” (Fig. 7a). Likewise the winters 1992/93 and 1996/97 combine to form a second cluster, denoted “type B.” At the next level of the cluster tree, the unusual winter 1995/96 combines with type B to form an extended cluster “type B+” (Fig. 7b) similar to type B. Type A is characterized in high latitudes by relatively strong flow in early winter and relatively weak flow in midwinter. Type B or B+ is characterized in high latitudes by relatively weak flow in early winter and relatively strong flow in midwinter. The winters 1993/94 and 1997/98 combine to form a third cluster, denoted “type C,” which is similar to type A, with deceleration in high latitudes after solstice. The winter 1998/99 is obviously similar to type C and combines at the next level to form an extended cluster, “type C+” (Fig. 7c). The three clusters each contain a sudden deceleration of the subtropical mesospheric jet, followed by redevelopment of weaker westerlies in midlatitudes;

they differ in the sequence of events at high latitudes. In type B or B+, westerlies persist through solstice and are mildly attenuated about a month after the midpoint of the composite. In type A, the subtropical deceleration extends to high latitudes, followed by a brief westerly reacceleration there, and then strong easterly acceleration. This easterly anomaly appears about a month after the subtropical deceleration. In type C or C+, the subtropical deceleration extends to high latitudes within about 10 days, followed by a slow but persistent westerly acceleration over the next 30 days.

Comparing types A and B+, the subtropical deceleration and polar deceleration after 30 days are both stronger in A. This is also true of type A relative to C+, suggesting that the intensities of the two deceleration events, separated by as much as 30 days, are somehow related.

The 8-yr average blends together features seen in the individual clusters (Fig. 7d). On average, the high-latitude easterly anomaly occurs about a month after the subtropical deceleration. The poleward progression of deceleration is not continuous but rather occurs in two stages. At the time of the subtropical deceleration, the high-latitude flow briefly accelerates. Over the next 30

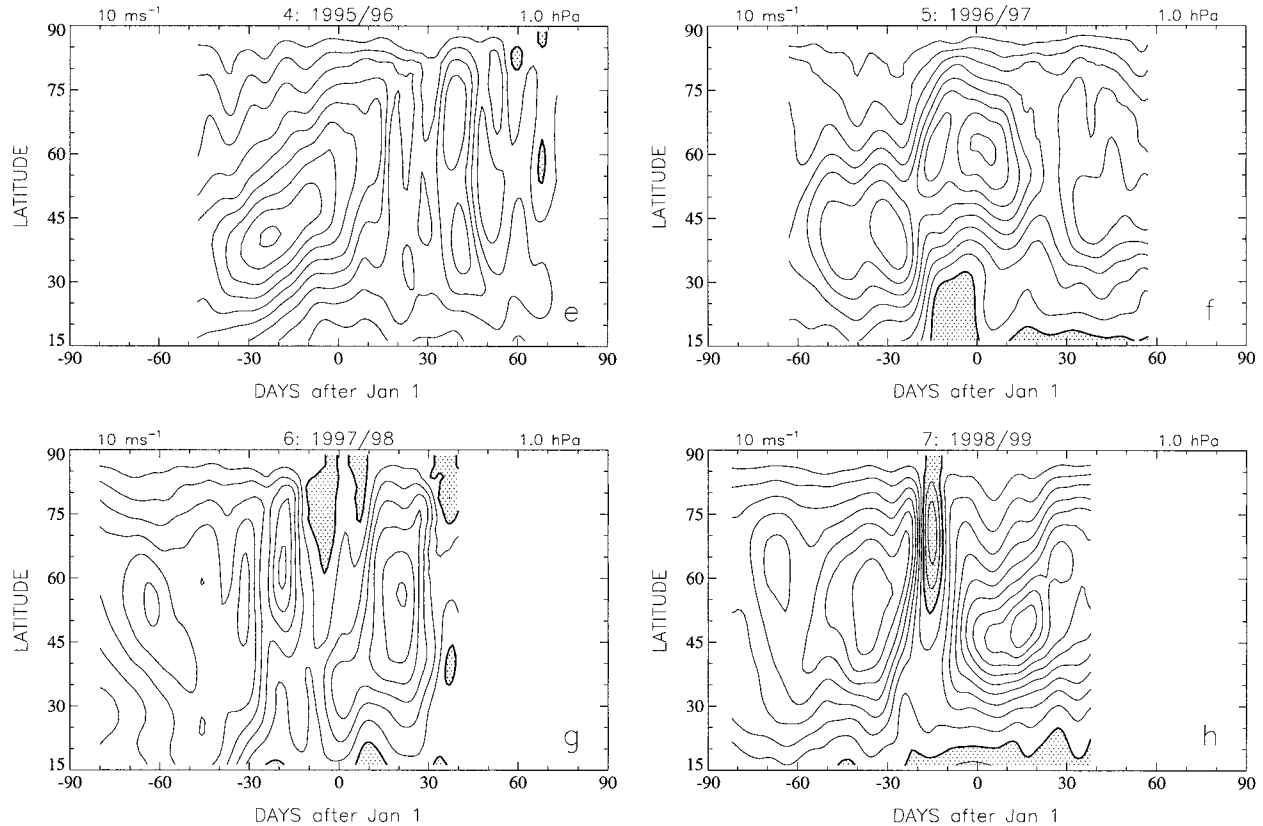


FIG. 6. (Continued)

days, during the time of high-latitude deceleration, westerlies are reestablished in midlatitudes.

#### b. Composites with respect to SMJ-*m* peak

The contrasting mean flow evolution described above is also seen in the behavior of individual EOFs of low-pass filtered data. Principal component time series of intraseasonal modes composited according to their cluster membership are shown in Fig. 8 for types A and B+ and for all years combined. These series were converted to an index (in units of  $\text{m s}^{-1}$ ) by multiplying the normalized principal component time series by the maximum value of dimensional rotated EOF, or in the case of dipole modes, by multiplying the principal component by the difference between values at the EOF's two extrema. The contribution of each EOF to the dimensional zonal wind at a single point (or to the difference between two points) was obtained thereby, as shown in the figure. The first series, at the top, shows the contribution attributable to the SMJ-d mode as the difference between EOF data at  $23.75^{\circ}\text{N}$ , 1.46 hPa, and  $48.75^{\circ}\text{N}$ , 1.46 hPa. The second series shows the contribution attributable to the SMJ-m mode at  $36.25^{\circ}\text{N}$ , 1.0 hPa, which lags the first by about 30 days. By definition, this mode is largest negative at zero lag. The third series is the negative of the first series, lagging

the second series by about 20 days. The phase lag implies poleward propagation of an easterly anomaly in the upper stratosphere. Results for type C+ (not shown) are similar to those of A. The two categories A, B+ differ significantly in the evolution of the PNJ-*m* mode, contained in the fourth series, showing the contribution from this mode at  $66.25^{\circ}\text{N}$ , 3.16 hPa. Type A indicates strong deceleration of the polar night jet at positive lags, while type B+ indicates a relatively weak polar night jet in early winter followed by a persistent westerly anomaly thereafter. The fifth series shows the contribution from the PNJ-d mode as the difference between  $71.25^{\circ}\text{N}$ , 21.5 hPa, and  $58.75^{\circ}\text{N}$ , 1.0 hPa. In the B+ composite, near zero lag, vertical shear is anomalously strong between the middle and upper stratosphere.

Another illustration of the two composites is provided in Fig. 9, showing the mean zonal wind at zero lag and at two times on either side of zero, when the difference between composites is large. In early winter ( $-40$  days), the jet axis in type B+ is displaced  $10^{\circ}$ – $20^{\circ}$  equatorward relative to type A. In the region sampled by the PNJ-*m* mode, therefore, the polar night jet is stronger by about  $10 \text{ m s}^{-1}$  in type A and tilts equatorward with height. At zero lag, the profiles are similar but vertical shear is stronger in B+. At  $+30$  days the polar flow in type A has broken down, with a weak vortex detached from the subtropical jet, while in type B+ the vortex remains

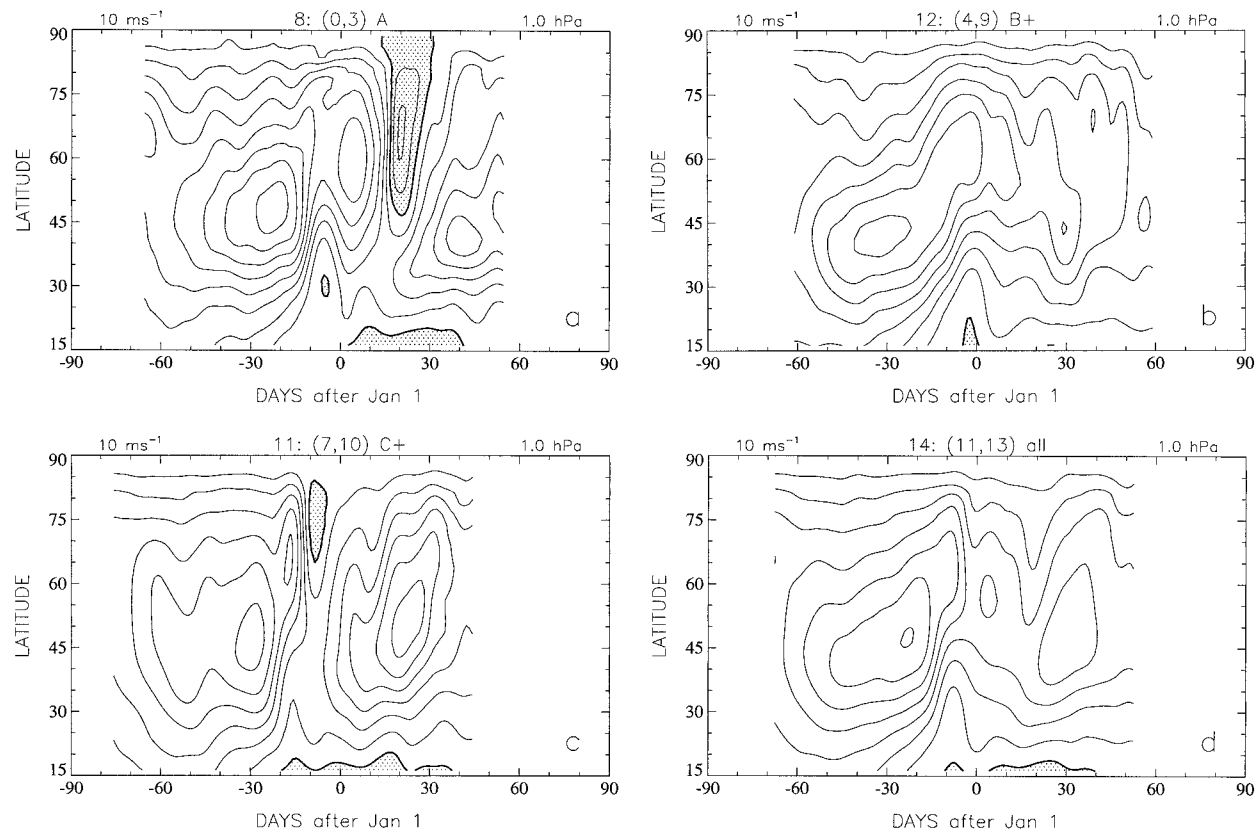


FIG. 7. Composites of zonally averaged zonal wind at 1.0 hPa obtained from cluster analysis. (a) Type A; (b) type B+; (c) type C+; (d) average of all years. The years used in the composite are indicated on the title row (see Figs. 5, 6). Cluster 9 represents the combination of 1 and 5; cluster 10 represents the combination of 2 and 6. Shading indicates negative values; contour interval is  $10 \text{ m s}^{-1}$ .

intact, extending into the upper stratosphere. The jet configuration in type A in early winter is more favorable for vertical propagation of planetary waves than that of type B+, which may help to explain the polar deceleration of type A in midwinter.

Returning to Fig. 8 it can be seen that the poleward propagation of stratopause anomalies continues at positive lags in type A but is slowed down and less apparent in type B+. Perhaps the most remarkable feature of Fig. 8a is the steady poleward and downward propagation<sup>2</sup> of an easterly anomaly exemplified in the top four curves. In Fig. 8b this feature is not apparent after solstice. Rather, there is slower poleward and downward propagation of a westerly anomaly throughout the figure. When all years are combined, the poleward and downward propagation of westerly and easterly anomalies is clearly seen, separated by about 30 days (Fig. 8c). The impression gained is that the difference between composites cannot be attributed to any difference in the initial poleward propagation along the stratopause

but is rather attributable to, or associated with, differences in the structure and evolution of the polar night jet. After the solstice, poleward propagation along the stratopause may be affected by the state of the polar vortex.

### c. Interpretation

The poleward/downward propagation of mean zonal wind anomalies in the northern winter stratosphere, highlighted in recent literature (e.g., Kuroda and Kodera 1999), is somewhat variable from year to year, mainly due to the high-latitude flow. Poleward propagation of anomalies along the stratopause is fairly regular, but the timing of deceleration events in the polar region is quite irregular. Three distinct patterns of behavior are evident here; it is possible that more patterns will emerge in a longer dataset.

A simple interpretation in terms of the dynamics of Rossby wave propagation and breaking may help to explain the contrast between the regular poleward propagation of mean zonal wind anomalies along the stratopause and the irregular behavior of the polar vortex. In each winter there is a finite amount of planetary wave activity that, even if relatively small in some winters,

<sup>2</sup> The rate of propagation appears uniform in low-pass filtered data, but in lightly filtered data the easterly deceleration of type A is temporarily interrupted by westerly reacceleration.

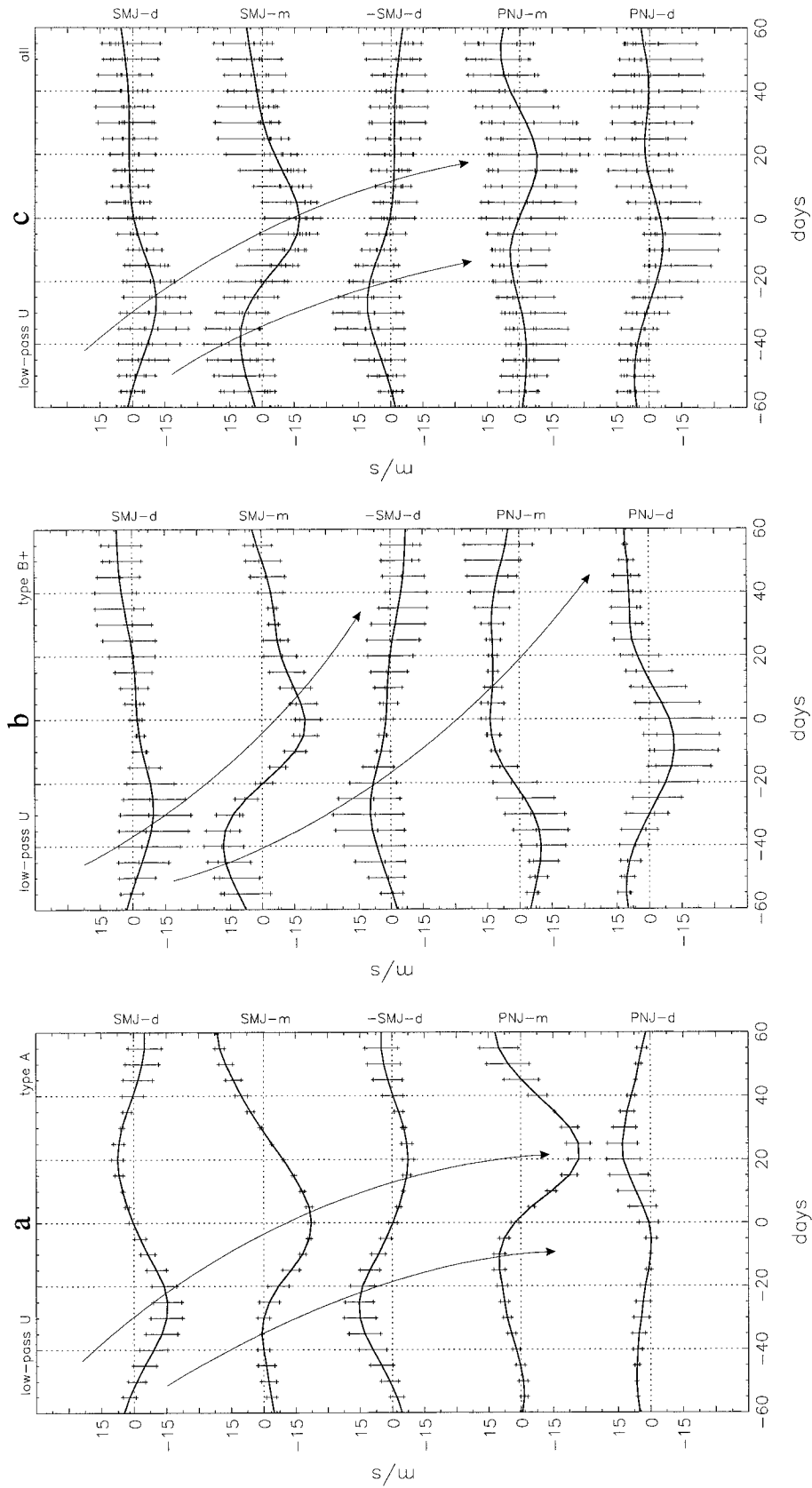


FIG. 8. Composites of zonal wind anomalies attributable to intraseasonal modes of the Northern Hemisphere stratosphere derived from principal component time series (see text). Zero lag corresponds to the maximum midwinter value of SMJ-m time series, indicating the time of largest easterly anomaly attributable to this mode near northern winter solstice. Vertical bars show the range of values in individual years. (a) Type A; (b) type B+; (c) all years.

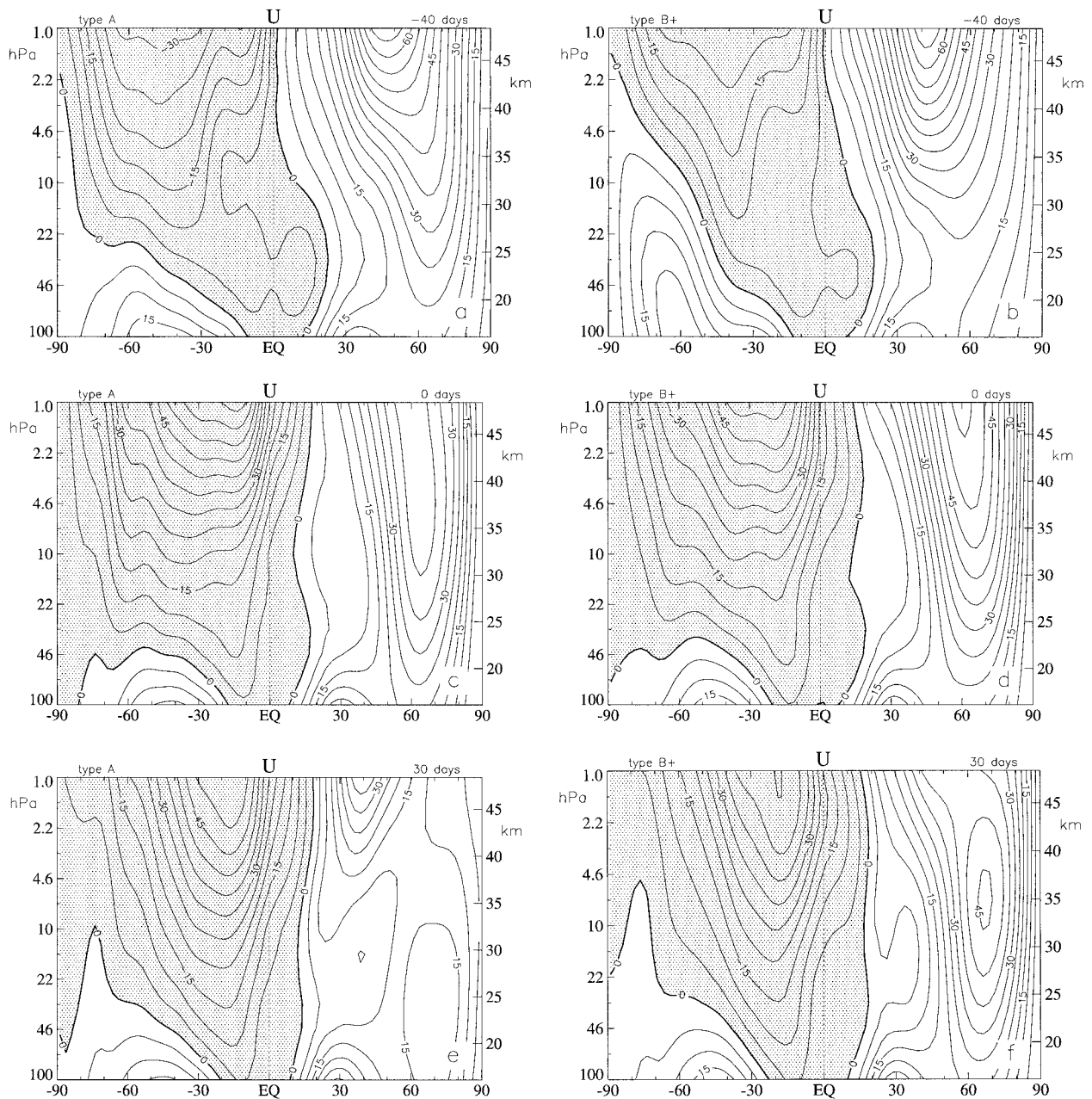


FIG. 9. Latitude–height cross section of mean zonal wind composites for type A (a), (c), (e) and type B+ (b), (d), (f) events, at various lags with respect to the maximum midwinter value of SMJ-m principal component time series. Shading indicates negative values; contour interval is  $5 \text{ m s}^{-1}$ .

grows to sufficient amplitude at upper levels so as to cause breaking at the edge of the polar vortex, accompanied by contraction of the vortex and poleward propagation of the vortex edge (Dunkerton and Delisi 1986). The timing and amount of significant wave activity, on the other hand, vary considerably from year to year. Thus, the timing and intensity of polar warmings vary from year to year. It would be illogical to suppose that the irregular variation of the polar flow is caused by the

*regular* poleward propagation of stratopause anomalies; the polar variability rather must be associated with the underlying tropospheric forcing and/or the dynamics of the polar vortex itself. Thus the observed poleward and downward progression of anomalies—manifest in various ways in this dataset and arguably present in other datasets—should be interpreted with caution. First, we have seen that the character and rate of propagation differ considerably between types A and B. These two

clusters exemplify relatively disturbed and undisturbed winters, respectively. Second, the direction of anomaly propagation says nothing about the direction of causality, nor does it suggest that the lower atmosphere is influenced by the upper atmosphere. It is expected that upward- and equatorward-propagating planetary waves cause irreversible changes in the mean state, altering the conditions for wave propagation in such a way as to draw mean-flow anomalies poleward and downward.

## 6. Conclusions

The variability of zonally averaged stratospheric circulation was examined using daily gridded analyses from the U.K. Met. Office (UKMO) for 1991–99, corresponding to the period observed by the *Upper Atmosphere Research Satellite (UARS)*. Application of rotated principal component analysis to the dataset revealed dominant modes of variability consisting of annual, semiannual, and quasi-biennial oscillations, together with intraseasonal and interannual variability in the winter hemisphere. The UKMO data are considered reliable for the purpose of identifying the temporal variation of these phenomena, although in the tropical upper stratosphere the quasi-biennial and semiannual oscillations are too weak. In the upper stratosphere during northern winter, we observe poleward propagating zonal wind anomalies at the stratopause and a sudden deceleration of the subtropical mesospheric jet in each midwinter. The high-latitude flow is more variable, and the data suggest two contrasting types of wintertime evolution in the polar stratosphere. One (types A, C) is characterized in high latitudes by relatively strong flow in early winter and a significantly weakened flow after solstice, the other (type B) by relatively weak flow in early winter and a strong positive flow anomaly after solstice. In both, the subtropical deceleration is accompanied by high-latitude acceleration. In the second type, polar westerlies remain long after solstice, decaying gradually, while in the first type, polar easterlies appear after 10–30 days. In two winters of the first type, the subtropical deceleration is unusually abrupt, followed by brief reacceleration of the polar vortex and a spectacular breakdown after 30 days.

Multivariate EOF analysis incorporating temperature data separates deceleration events in northern winter affecting the subtropical jet, with midlatitude warming, from those affecting the polar night jet, with polar warming. The location of maximum warming is presumably also the location of maximum anomalous subsidence during these events.

Our study demonstrates that the most interesting dynamics of the middle atmosphere occur in the upper stratosphere and lower mesosphere where variance is maximum. Only two phenomena contribute to variance maxima in the middle stratosphere: the tropical QBO and persistence of the south polar vortex in Southern Hemisphere spring. For the last 15 years, middle-at-

mosphere research has emphasized the lower stratosphere, where important chemical and physical processes are sensitive to the colder temperatures of this region (dehydration, denitrification, aerosol or polar stratospheric cloud (PSC) formation, heterogeneous chemistry, and ozone depletion). From a purely dynamical viewpoint, this emphasis on the lower stratosphere is unwarranted; most of the action is at higher altitudes, where planetary waves break down violently, barotropic and inertial instabilities occur, and mean flows evolve rapidly.

This paper discusses basic elements of zonally averaged dynamics, emphasizing slow variations on a timescale of a month or longer. Several of these variations are well known, as summarized in Belmont et al. (1974); our EOF analysis is complementary to traditional harmonic analysis. On intraseasonal timescales the low-pass filtered data provide a smooth description of phenomena that, in reality, display more complicated behavior on shorter timescales (Fig. 6). The analysis is not exhaustive but illustrates the usefulness of the technique, which if applied with better discrimination, could reveal additional features in the data (e.g., Baldwin and Tung 1994).

Evidence of intraseasonal variations in the northern winter suggests an interpretation in terms of planetary wave, mean-flow interaction. If ideas put forth to explain the evolution of the polar vortex and surf zone in the middle stratosphere (McIntyre and Palmer 1984; Butchart and Remsberg 1986) apply equally well near the stratopause, as they presumably do (Dunkerton and Delisi 1986), then the poleward propagation of mean zonal wind anomalies at this altitude can be associated with erosion of the polar vortex and poleward propagation of vortex edge. These processes are expected to occur more rapidly at the stratopause than in the middle stratosphere on account of the lower atmospheric density and growth of planetary waves with height. Radiative relaxation is also faster at this altitude, contributing to rapid reacceleration of the flow. A sudden deceleration of the subtropical mesospheric jet has been observed thus far in each UKMO winter, suggesting that the behavior in December 1978 documented previously (Dunkerton and Delisi 1985a) is not unusual, but a dependable feature at this altitude. Given that planetary waves of zonal wavenumber 1 grow with height under normal westerly flow conditions, the breakdown of upper stratosphere flow in midwinter and the accompanying “transition to turbulence” seem more likely than the breakdown of polar vortex in the middle and lower stratosphere; indeed, major warmings below 10 hPa do not occur in every year (Labitzke 1987).

Interannual variations of planetary wave activity, polar vortex strength, and lower stratospheric temperature have been shown to affect the behavior of trace chemical constituents during the *UARS* observing period. O’Sullivan and Dunkerton (1997) observed a more vigorous lateral mixing due to planetary waves entering

the subtropics in the first *UARS* northern winter, relative to that of the second winter, suggesting a role of the QBO in modulating the equatorward propagation and breakdown of the waves. These two winters afford good illustrations of type A and B behavior, respectively, associated with relatively disturbed and undisturbed conditions in mid- to late winter. Record cold temperatures in the 1995/96 northern winter were noted by Manney et al. (1996) as setting the stage for PSC formation and a remarkable depletion of ozone in the Arctic. The following winter 1996/97 was even more remarkable as the polar vortex survived into late April and was unusually strong, cold, and symmetric (Coy et al. 1997), once again leading to record ozone depletion (Newman et al. 1997; Manney et al. 1997; Kreher et al. 1999; Hansen and Chipperfield 1999). Planetary wave transport was unusually weak in late winter 1996/97 (Coy et al. 1997). These two winters—especially the second—illustrate type B behavior characterized by relatively weak flow in early winter and relatively strong flow in mid- to late winter. At the time of this writing, an unusually early major warming has been observed in the 1998/99 winter (Manney et al. 1999) followed by nearly record cold temperatures in February 1999 but was interrupted by another warming in late February. A pattern of compensation between relatively disturbed and undisturbed conditions within each winter—some with disturbed conditions early, and some late—seems to characterize most of the northern winters in the *UARS* observing period and is seen in a much longer record (Dunkerton and Baldwin 1991). The preference for one sequence over the other is important to stratospheric chemistry because, for example, a coincidence of cold temperature, PSC formation, and sunlight in late winter would be favorable for ozone depletion involving heterogeneous chemistry. Similarly, persistence of the polar vortex into spring might favor the depletion of ozone due to nitrogen chemistry as argued by Hansen and Chipperfield (1999). The timing of extreme cold is important: if occurring in early winter and followed by relatively warm conditions in late winter, ozone depletion is less likely.

This interplay between dynamics and chemistry underscores the need for a better understanding of the dynamical variability and seasonal evolution of the middle atmosphere. The state of the polar vortex after solstice evidently depends on its state within the preceding months, and its temporal evolution therefore cannot be described as a random walk.

Routine analysis of the stratosphere and lower mesosphere and the eventual extension of assimilation methods to the upper mesosphere will provide a new opportunity to investigate the entire middle atmosphere, from a climatological perspective, with dynamically consistent data. Additional years of data will increase the significance of results obtained from principal component analysis and will provide a more detailed and useful classification of wintertime flow evolution.

*Acknowledgments.* UKMO data were obtained from the British Atmospheric Data Center with the assistance of Lesley Gray. Comments of Steve Pawson and two anonymous reviewers were helpful for the reorganization of this paper and a companion paper. This research was supported by the National Aeronautics and Space Administration, Contracts NAS1-96071, NAS1-99130, and NAS5-98078.

#### REFERENCES

- Andrews, D. G., J. R. Holton, and C. B. Leovy, 1987: *Middle Atmosphere Dynamics*. Academic Press, 489 pp.
- Baldwin, M. P., and K. K. Tung, 1994: Extratropical QBO signals in angular momentum and wave forcing. *Geophys. Res. Lett.*, **21**, 2717–2720.
- , and T. J. Dunkerton, 1999: Propagation of the Arctic Oscillation from the stratosphere to the troposphere. *J. Geophys. Res.*, **104**, 30 937–30 946.
- , X. Cheng, and T. J. Dunkerton, 1994: Observed correlations between winter-mean tropospheric and stratospheric circulation anomalies. *Geophys. Res. Lett.*, **21**, 1141–1144.
- Belmont, A. D., D. G. Dartt, and G. D. Nastrom, 1974: Periodic variations in stratospheric zonal wind from 20–65 km, at 80N to 70S. *Quart. J. Roy. Meteor. Soc.*, **100**, 203–211.
- , —, and —, 1975: Variations of stratospheric zonal winds, 20–65 km, 1961–1971. *J. Appl. Meteor.*, **14**, 585–594.
- Bretherton, C. S., C. Smith, and J. M. Wallace, 1992: An intercomparison of methods for finding coupled patterns in climate data. *J. Climate*, **5**, 541–560.
- Butchart, N., and E. E. Remsberg, 1986: The area of the stratospheric polar vortex as a diagnostic for tracer transport on an isentropic surface. *J. Atmos. Sci.*, **43**, 1319–1339.
- Cheng, X., and T. J. Dunkerton, 1995: Orthogonal rotation of spatial patterns derived from singular value decomposition analysis. *J. Climate*, **8**, 2631–2643.
- Coy, L., E. R. Nash, and P. A. Newman, 1997: Meteorology of the polar vortex: Spring 1997. *Geophys. Res. Lett.*, **24**, 2693–2696.
- Dunkerton, T. J., 1997: The role of gravity waves in the quasi-biennial oscillation. *J. Geophys. Res.*, **102**, 26 053–26 076.
- , 2000: Quasi-biennial and subbiennial variations of stratospheric trace constituents derived from HALOE observations. *J. Atmos. Sci.*, **58**, 7–25.
- , and D. P. Delisi, 1985a: The subtropical mesospheric jet observed by the Nimbus 7 Limb Infrared Monitor of the Stratosphere. *J. Geophys. Res.*, **90**, 10 681–10 692.
- , and —, 1985b: Climatology of the equatorial lower stratosphere. *J. Atmos. Sci.*, **42**, 376–396.
- , and —, 1986: Evolution of potential vorticity in the winter stratosphere of January–February 1979. *J. Geophys. Res.*, **91**, 1199–1208.
- , and M. P. Baldwin, 1991: Quasi-biennial modulation of planetary-wave fluxes in the Northern Hemisphere winter. *J. Atmos. Sci.*, **48**, 1043–1061.
- , and D. P. Delisi, 1997: Interaction of the quasi-biennial oscillation and stratopause semiannual oscillation. *J. Geophys. Res.*, **102**, 26 107–26 116.
- Eder, B. K., S. K. LeDuc, and J. E. Sickles II, 1999: A climatology of total ozone mapping spectrometer data using rotated principal component analysis. *J. Geophys. Res.*, **104**, 3691–3709.
- Garcia, R. R., T. J. Dunkerton, R. S. Lieberman, and R. A. Vincent, 1997: Climatology of the semiannual oscillation of the tropical middle atmosphere. *J. Geophys. Res.*, **102**, 26 019–26 032.
- Gray, L. J., and J. M. Russell III, 1999: Interannual variability of trace gases in the subtropical winter stratosphere. *J. Atmos. Sci.*, **56**, 977–993.
- Hamilton, K., 1984: Mean wind evolution in the tropical lower stratosphere. *J. Atmos. Sci.*, **41**, 2113–2125.

- Hansen, G., and M. P. Chipperfield, 1999: Ozone depletion at the edge of the Arctic polar vortex 1996/1997. *J. Geophys. Res.*, **104**, 1837–1846.
- Hitchman, M. H., and C. B. Leovy, 1986: Evolution of the zonal mean state in the equatorial middle atmosphere during October 1978–May 1979. *J. Atmos. Sci.*, **43**, 3159–3176.
- Holton, J. R., and H.-C. Tan, 1980: The influence of the equatorial quasi-biennial oscillation on the global circulation at 50 mb. *J. Atmos. Sci.*, **37**, 2200–2208.
- Kim, K.-Y., and Q. Wu, 1999: A comparison study of EOF techniques: Analysis of nonstationary data with periodic statistics. *J. Climate*, **12**, 185–199.
- Kreher, K., G. E. Bodeker, H. Kanzawa, H. Nakane, and Y. Sasano, 1999: Ozone and temperature profiles measured above Kiruna inside, at the edge of, and outside the Arctic polar vortex in February and March 1997. *Geophys. Res. Lett.*, **26**, 715–718.
- Kuroda, Y., and K. Kodera, 1999: Role of planetary waves in the stratosphere–troposphere coupled variability in the northern hemisphere winter. *Geophys. Res. Lett.*, **26**, 2375–2378.
- Labitzke, K., 1981: Stratospheric–mesospheric midwinter disturbances: A summary of observed characteristics. *J. Geophys. Res.*, **86**, 9665–9678.
- , 1987: Sunspots, the QBO, and the stratospheric temperature in the north polar region. *Geophys. Res. Lett.*, **14**, 535–537.
- Livezey, R. E., and T. M. Smith, 1999: Covariability of aspects of North American climate with global sea surface temperatures on interannual to interdecadal timescales. *J. Climate*, **12**, 289–302.
- Manney, G. L., M. L. Santee, L. Froidevaux, J. W. Waters, and R. W. Zurek, 1996: Polar vortex conditions during the 1995–1996 Arctic winter: Meteorology and MLS ozone. *Geophys. Res. Lett.*, **23**, 3203–3206.
- , L. Froidevaux, M. L. Santee, R. W. Zurek, and J. W. Waters, 1997: MLS observations of Arctic ozone loss in 1996–1997. *Geophys. Res. Lett.*, **24**, 2697–2700.
- , W. A. Lahoz, R. Swinbank, A. O'Neill, P. M. Connaw, and R. W. Zurek, 1999: Simulation of the December 1998 stratospheric major warming. *Geophys. Res. Lett.*, **26**, 2733–2736.
- McIntyre, M. E., and T. N. Palmer, 1984: The “surf zone” in the stratosphere. *J. Atmos. Terr. Phys.*, **46**, 825–849.
- Newman, P. A., J. F. Gleason, R. D. McPeters, and R. S. Stolarski, 1997: Anomalously low ozone over the Arctic. *Geophys. Res. Lett.*, **24**, 2689–2692.
- Nigam, S., 1990: On the structure of variability of the observed tropospheric and stratospheric zonal-mean zonal wind. *J. Atmos. Sci.*, **47**, 1799–1813.
- Ortland, D. A., 1997: Rossby wave propagation into the tropical stratosphere observed by the High Resolution Doppler Imager. *Geophys. Res. Lett.*, **24**, 1999–2002.
- O’Sullivan, D. J., and T. J. Dunkerton, 1994: Seasonal development of the extratropical QBO in a numerical model of the middle atmosphere. *J. Atmos. Sci.*, **51**, 3706–3721.
- , and ———, 1997: The influence of the quasi-biennial oscillation on global constituent distributions. *J. Geophys. Res.*, **102**, 21 731–21 743.
- Plumb, R. A., and R. C. Bell, 1982: A model of the quasi-biennial oscillation on an equatorial beta-plane. *Quart. J. Roy. Meteor. Soc.*, **108**, 335–352.
- Randel, W. J., F. Wu, J. M. Russell III, A. Roche, and J. W. Waters, 1998: Seasonal cycles and QBO variations in stratospheric CH<sub>4</sub> and H<sub>2</sub>O observed in UARS HALOE data. *J. Atmos. Sci.*, **55**, 163–185.
- , ———, ———, and J. Waters, 1999a: Space–time patterns of trends in stratospheric constituents derived from UARS measurements. *J. Geophys. Res.*, **104**, 3711–3727.
- , ———, R. Swinbank, J. Nash, and A. O'Neill, 1999b: Global QBO circulation derived from UKMO stratospheric analyses. *J. Atmos. Sci.*, **56**, 457–474.
- Ray, E. A., M. J. Alexander, and J. R. Holton, 1998: An analysis of the structure and forcing of the equatorial semiannual oscillation in zonal wind. *J. Geophys. Res.*, **103**, 1759–1774.
- Reber, C. A., C. E. Trevathan, R. J. McNeal, and M. R. Luther, 1993: The Upper Atmosphere Research Satellite (UARS) mission. *J. Geophys. Res.*, **98**, 10 643–10 647.
- Russell, J. M., III, and Coauthors, 1993: The Halogen Occultation Experiment. *J. Geophys. Res.*, **98**, 10 777–10 797.
- Swinbank, R., and A. O'Neill, 1994: A stratosphere–troposphere data assimilation system. *Mon. Wea. Rev.*, **122**, 686–702.
- Thompson, D. W. J., and J. M. Wallace, 1998: The Arctic Oscillation signature in the wintertime geopotential height and temperature fields. *Geophys. Res. Lett.*, **25**, 1297–1300.
- , and ———, 2000: Annular modes in the extratropical circulation. Part I: Month-to-month variability. *J. Climate*, **13**, 1000–1016.
- Weickmann, K. M., and R. M. Chervin, 1988: The observed and simulated atmospheric seasonal cycle. Part I: Global wind field modes. *J. Climate*, **1**, 265–289.